Transcriptional pattern enriched for synaptic signaling is associated with shorter survival of patients with high-grade serous ovarian cancer

Arkajyoti Bhattacharya [#,1],PhD, Thijs S. Stutvoet [#,1],MD, PhD, Mirela Perla[#,1],MSc, Stefan Loipfinger[1], MSc, Mathilde Jalving[1],MD, PhD, Anna K.L. Reyners[1],MD, PhD, Paola D. Vermeer[2], PhD, Ronny Drapkin[3],MD, PhD, Marco de Bruyn[4],PhD, Elisabeth G.E. de Vries[1],MD, PhD, Steven de Jong[1],PhD, Rudolf S.N. Fehrmann [*,1],MD, PhD

[1]Department of Medical Oncology, University Medical Center Groningen, University of Groningen, Groningen, the Netherlands, [2]Cancer Biology and Immunotherapies Group, Sanford Research, Sioux Falls, SD, [3]Penn Ovarian Cancer Research Center and Basser Center for BRCA, University of Pennsylvania, Perelman School of Medicine, Philadelphia, PA, [4]Department of Obstetrics and Gynecology, University Medical Center Groningen, University of Groningen, Groningen, the Netherlands

[#] Contributed equally

[*]**Corresponding author:**

Rudolf S.N. Fehrmann, MD, PhD

Department of Medical Oncology, University Medical Center Groningen

P.O. Box 30.001, 9700 RB Groningen, the Netherlands

Tel. +31503612821, Fax +31503614862

E-mail: r.s.n.fehrmann@umcg.nl

Abstract

Background: Bulk transcriptomic analyses of high-grade serous ovarian cancer (HGSOC) so far have not uncovered potential drug targets, possibly because subtle, disease-relevant transcriptional patterns are overshadowed by dominant, non-relevant ones. Our aim was to uncover disease-outcome-related patterns in HGSOC transcriptomes that may reveal novel drug targets.

Method: Using consensus-independent component analysis, we dissected 678 HGSOC transcriptomes of systemic therapy naïve patients—sourced from public repositories—into statistically independent transcriptional components (TCs). To enhance c-ICA's robustness, we added 447 transcriptomes from non-serous histotypes, low-grade serous, and non-cancerous ovarian tissues. Cox regression and survival tree analysis were performed to determine the association between TC activity and overall survival (OS). Finally, we determined the activity of the OS-associated TCs in 11 publicly available spatially resolved ovarian cancer transcriptomes.

Results: We identified 374 TCs, capturing prominent and subtle transcriptional patterns linked to specific biological processes. Six TCs, age, and tumor stage stratified patients with HGSOC receiving platinum-based chemotherapy into ten distinct OS groups. Three TCs were linked to copy-number alterations affecting expression levels of genes involved in replication, apoptosis, proliferation, immune activity, and replication stress. Notably, the TC identifying patients with the shortest OS captured a novel transcriptional pattern linked to synaptic signaling, which was active in tumor regions within all spatially resolved transcriptomes.

Conclusion: The association between a synaptic signaling-related TC and OS supports the emerging role of neurons and their axons as cancer hallmark-inducing constituents of the tumor microenvironment. These constituents might offer a novel drug target for patients with HGSOC.

Keywords: high-grade serous ovarian cancer (HGSOC), synaptic signaling, consensus independent component analysis, transcriptome

Background

Epithelial ovarian cancer encompasses five primary histological subtypes, with high-grade serous ovarian carcinoma (HGSOC) constituting about 75% of all cases (1). The standard treatment for HGSOC diagnosed at stage IIB and beyond involves a combination of surgery and chemotherapy, primarily using platinum-based compounds and taxanes (2,3). While initial chemotherapy results in tumor response in most patients with HGSOC, there is a very high recurrence rate (4). The addition of poly-ADP ribose polymerase and vascular endothelial growth factor A inhibitors to chemotherapy for subsets of patients currently results in a 5-year disease-specific overall survival (OS) rate of approximately 45% for patients with HGSOC. This rate has hardly improved in the last three decades (5–8). Therefore, new insights into the complex biology underlying HGSOC are urgently needed to develop more effective treatment strategies.

Previous studies using bulk transcriptomes of patients with HGSOC have identified expression-based molecular subtypes. However, these subtypes did not provide insights that have translated into novel drug targets (9–11). A common limitation of such studies is their reliance on bulk transcriptomes, containing both tumor cells and tumor microenvironment (TME) components, thus reflecting the average transcriptional patterns of the combination of all biological processes present in the tumors. This averaging often masks subtle transcriptional patterns pivotal to understanding HGSOC biology, especially when these are overshadowed by dominant patterns from other less relevant (non-)biological processes (12). Consensus-independent component analysis (c-ICA) offers an alternative by decomposing such bulk transcriptomes into statistically independent transcriptional patterns (i.e., transcriptional components; TCs)(13,14). This approach reveals both dominant and subtle patterns and provides a measure of TC activity for each sample (15).

In the present study, our aim was to utilize c-ICA to dissect HGSOC transcriptomes to identify as many TCs associated with patient OS as possible, which could reveal potential novel drug targets.

Methods

See Supplementary methods for the extended methods.

Data acquisition

Raw microarray bulk transcriptomes and clinicopathological details for patients with HGSOC, low-grade serous ovarian cancer (LGSOC), non-serous ovarian cancer, and benign ovarian tissues were sourced from the Gene Expression Omnibus (GEO)(16). We exclusively utilized transcriptomes generated from primary tumor samples. Our analysis was confined to samples on the Affymetrix HG-U133 Plus 2.0 platform (GEO accession identifier: GPL570) and excluded cell line samples. The datasets were pre-processed, and quality controlled as previously described (17). Furthermore, for comprehensive analyses, we incorporated transcriptomes from five distinct resources: the Cancer Cell Line Encyclopedia (CCLE, n = 969), Genomics of Drug Sensitivity in Cancer (GDSC, n = 959), Gene Expression Omnibus (GEO, n = 13,810), and The Cancer Genome Atlas (TCGA, n = 8,150), and spatially resolved transcriptomes from 10xGenomics (16,18–20).

Consensus-independent component analysis (c-ICA)

To preprocess the bulk transcriptome data, we applied a whitening transformation to prepare it for subsequent analysis. Consensus-ICA was conducted as described previously (Knapen et al., 2024). The output of an c-ICA includes two matrices: (i) transcriptional components (TCs) with gene weights, where each weight within the TC represents both the

97 direction and magnitude of its effect on the expression levels of each gene, and (ii) a
98 consensus mixing matrix (MM) with its coefficients representing the activity scores of TCs
99 across samples. **Survival analysis**

100 To discern the relationship between TC activity and patient OS, a univariate Cox proportional
101 hazards analysis was conducted on a select group of patients with available follow-up data (*n*
102 = 541, Supplementary Table S1). In addition, a multivariate Cox proportional hazards analysis
103 was carried out, including covariates such as age, stage, debulking status, and tumor grade.
104 This latter analysis was based on a subset of patients with comprehensive clinicopathological
105 data available (*n* = 373, Supplementary Table S1). We implemented a multivariate
106 permutation framework encompassing 10,000 permutations to mitigate the risk of false
107 discoveries. We established the acceptable false discovery rate (FDR) at 1%, maintaining an
108 80% confidence level, applicable for both the univariate and multivariate analyses.

109

110 **Survival tree analysis**

111 We performed a survival tree analysis to delineate groups of patients with HGSOC treated
112 with platinum-based chemotherapy based on distinct transcriptional and clinicopathological
113 attributes. The analysis utilized activities of TCs associated with OS (either from univariate or
114 multivariate survival analysis as mentioned in supplementary methods) in conjunction with
115 relevant clinicopathological factors, such as age, tumor stage, debulking status, and grade, as
116 potential classifiers. We divided patients into two subsets using every plausible cut-off point
117 for each classifier and compared the resulting survival curves employing the log-rank
118 statistic. Consequently, the division was based on the most significant classifier at its optimal
119 cut-off based on the smallest p-value of the log-rank test mentioned above. This divisional
120 process was successfully reiterated on the derived subsets until any of the following

121 stipulated conditions was satisfied: *i*) the total patient count across both subsets fell below
122 50, *ii*) the collective number of uncensored events in both subsets was < 25, or *iii*) one of the
123 subsets contained < 17 patients. To gauge the stability of our classifiers, we performed
124 20,000 iterations, randomly selecting 80% of the patient group in each iteration. The
125 significance-based ranks of classifiers in these iterations were correlated with those from the
126 primary survival tree.
127

128 **Associating the identified transcriptional components with biological processes**

129 To discern the biological processes associated with the TCs, we adopted a multifaceted
130 approach encompassing *i*) Transcriptional Adaptation to Copy Number Alterations (TACNA)
131 profiling, targeting the identification of TCs that reflect the downstream implications of copy
132 number alterations (CNAs) on gene expression levels(21); *ii*) Execution of gene set
133 enrichment analysis (GSEA) for each TC, utilizing gene set collections (n = 16) from The
134 Human Phenotype Ontology (The Monarch Initiative), the Mammalian Phenotypes (Mouse
135 Genome Database), and the Molecular Signatures Database (MsigDB)(22,23); *iii*) The
136 formation of co-functionality networks on the top and bottom genes of each TC, achieved
137 using the GenetICA methodology, accessible via https://www.genetica-network.com(24). For
138 clusters comprising ≥ 5 genes, the enrichment of the predicted functionality was quantified.
139 This served as the foundation for determining the biological process associated with the TC
140 being examined.
141

142 **Cross-study transcriptional component projection**

143 To determine whether a biological process captured by an identified TC is also active in other
144 cancer types and to investigate if it is more active in tumor cells or in the tumour

145 microenvironment (TME), we collected raw expression profiles from multiple sources: the
146 Cancer Cell Line Encyclopedia (CCLE, *n* = 969), Genomics of Drug Sensitivity in Cancer (GDSC,
147 *n* = 959), Gene Expression Omnibus (GEO, *n* = 13,810), and The Cancer Genome Atlas (TCGA,
148 *n* = 8,150)(16,18–20). While the CCLE and GDSC datasets comprise cell line profiles across
149 many solid and hematologic malignancies, the GEO and TCGA datasets offer an extensive set
150 of bulk transcriptomes derived from patient samples spanning 27 tumor types. We pre-
151 processed the raw data as previously described (21). Next, we projected the TCs identified
152 via c-ICA onto the cell line expression profiles from CCLE and GDSC and the patient-derived
153 expression profiles from GEO and TCGA. This projection methodology has been described in
154 more detail previously (21). To identify potential variations in the activity scores of the TCs,
155 we compared the activity scores among cell lines and samples derived from patients within
156 all four repositories. We used an absolute activity score threshold of 0.05 for each TC to
157 pinpoint outlier cell lines and patient tumors with heightened activity.
158

159 **Determination of spatial transcriptomic profiles' significant activity locations for individual**
160 **transcriptional components**

161 To further assess whether a biological process captured by an identified TC is more active in
162 tumor cells or in the TME, we collected publicly available spatial resolved transcriptomic
163 profiles of ovarian cancer samples. Eight were sourced from GEO (study ID GSE211956), and
164 three were sourced from the public dataset repository of 10xGenomics (see supplementary
165 methods for details) generated using the 10xGenomics Visium platform. The samples were
166 from patients with HGSOC, serous papillary, and endometrioid ovarian cancer. Activity for
167 each TC across every location within the spatial samples was ascertained through the cross-
168 study projection methodology referred to in the previous method section (21). We

169 incorporated a permutation-driven approach to discern the markedly active areas within the
170 spatial samples for each TC. We derived a null distribution of activities for each TC-location
171 pairing by performing 3,000 permutations and subsequent projections. The p-value of each
172 observed TC activity quantifies the significance of the deviation of the TC activity at a given
173 location from its baseline null distribution. After this, we visualized the z-transformed p-
174 values using a heatmap, followed by obtaining colocalization scores for each combination of
175 TCs in the spatial transcriptomic profiles for each ovarian cancer sample (25). This
176 visualization aided in highlighting the areas with notable activity aligned against the stained
177 representation of the tissue sample.
178

179 ## Results

180 **An integrated data set containing 1,125 bulk transcriptomes from ovarian tissues**

181 We curated 1,193 bulk transcriptomes from the GEO, including patients with HGSOC, low-
182 grade serous ovarian cancer (LGSOC), non-serous ovarian cancer, and benign ovarian tissues
183 (16). These were extracted from 32 distinct studies and represented the entire spectrum of
184 ovarian cancer types, stages, and grades, and included 43 samples from non-malignant
185 ovarian tissue. Pre-processing, which included removing duplicates and quality checks,
186 culminated in a refined dataset of 1,125 samples (17). Supplementary Tables S1 and S2
187 provide detailed breakdowns of these samples, showcasing the comprehensive coverage of
188 ovarian cancer types, stages, and grades within this dataset. The ovarian cancer dataset
189 comprised bulk transcriptomes of patients with HGSOC (n = 678), other serous (n = 110),
190 endometrioid (n = 110), and clear-cell ovarian cancer samples (n = 96). Additionally, for 541
191 patients, comprehensive survival data was available, as well as additional clinicopathologic

192 information, including age, grade, stage, subtype, treatment schedule, and debulking status
193 for 373 patients (Fig. 1).
194
195 **Consensus-independent component analysis identifies 374 transcriptional components**
196 **(TCs)**
197 c-ICA on the 1,125 bulk transcriptomes revealed 374 independent TCs. Notably, 135 TCs
198 captured the impact of copy number alterations on gene expression levels. Each TC
199 displayed enrichment for at least one gene set from the 16 gene set collections, with an
200 absolute Z-score of more than two. For example, the number of enriched gene sets from the
201 Hallmark gene set collection in an individual TC ranged from zero to 28 enriched gene sets
202 (interquartile range 3 – 7). The median top Z score for Hallmark gene sets was 3.21 (range
203 1.55 – 37.54, interquartile range 2.6 – 4.25). A comprehensive database, including all TCs
204 and GSEA outcomes, has been made accessible at http://transcriptional-landscape-
205 ovarian.opendatainscience.net.
206 The activities of 13 TCs were associated with patient overall survival (OS) in a
207 univariate analysis, with an additional TC (TC166) identified in a multivariate analysis
208 accounting for age, stage, debulking, and tumor grade. Combined, these 14 OS-associated
209 TCs were enriched for gene sets associated with diverse biological processes and
210 clinicopathological characteristics, with four TCs capturing the effects of copy number
211 alterations on gene expression levels.
212
213 **The activities of six transcriptional components are associated with patient overall survival**
214 For a selected subset of 541 patients—including HGSOC, LGSOC, and non-serous ovarian
215 cancer—with available OS information (Supplementary Table S1), 13 TC activities displayed

216 an association with OS univariately (false discovery rate 5%, confidence level 80% in
217 permutation-based multiple testing framework Supplementary Table S3; Fig. 2). For patients
218 with serous ovarian cancer, treated with platinum-based therapy (*n* = 301, Supplementary
219 Table S1), lower activity of one additional TC (TC166) was associated with worse OS
220 independent of age, stage, debulking, and tumor grade (Supplementary Table S4).
221 Combined, these 14 OS-associated TCs were enriched for gene sets associated with diverse
222 biological processes and clinicopathological characteristics. Four of these TCs captured the
223 downstream effects of CNAs on gene expression levels (Fig. 2, Supplementary Fig. S1-S3).
224 Survival tree analysis identified ten groups of patients with platinum-treated HGSOC based
225 on the activity of six OS-associated TCs and the presence of two clinicopathological
226 characteristics, namely age and stage (Fig. 3, Supplementary Table S5, median robustness
227 statistic of survival tree = 0.52, interquartile range = 0.36 - 0.69). The survival tree
228 demonstrated good classification power (concordance statistic = 0.72, standard error =
229 0.021). As expected, patients were divided into separate survival groups based on stage (1/2
230 vs. 3/4) and age (<53.7 vs. ≥53.7 years). The most significant difference in OS was observed
231 between the cohorts with low and high TC121 activity (Supplementary Table S5). Patients
232 with high TC121 tumor activity exhibited the shortest OS, also observed for the subset of
233 patients with advanced-stage HGSOC (Supplementary Fig. S4, Supplementary Table S6).
234 Supplementary Fig. S5 indicates that TC121 activity is highest in patients with HGSOC
235 compared to other ovarian cancer subtypes. Notably, all subtypes contain subsets of
236 samples with elevated TC121 activity. These robust associations with OS for TC121 in these
237 two subsets of patients indicate the relevance of TC121, irrespective of stage.
238

239 **Distinct biological processes show enrichment in the transcriptional components**
240 **associated with overall survival**

241 Three of the six TCs associated with OS—TC166, TC247, and TC76—captured the effects of
242 CNAs on the expression levels of genes mapping to chromosome regions 13q12-q14, 11q13-
243 q14, and 9p13-p21, respectively (Supplementary Fig. S6, Supplementary Table S7) (6). The
244 higher activity of TC166 was associated with better OS, whereas the higher activities of
245 TC121, TC247, TC250, TC76, and TC146, were associated with worse OS. Among the 14 OS-
246 associated TCs, only TC166 showed a significant association with OS in an independent
247 cohort of patients with ovarian clear cell carcinoma (Bonferroni corrected p-value < 0.05; see
248 supplementary methods and Supplementary Table S8) (26) . The top genes from TC166 were
249 enriched for genes involved in replication and apoptosis. The chromosomal region 13q12-
250 q14 linked to the TC166, contains the tumor suppressor genes retinoblastoma 1 (*RB1*) and
251 Breast Cancer Type 2 Susceptibility Protein (*BRCA2*). Loss of heterozygosity of this
252 chromosomal region is frequently observed in both sporadic and hereditary serous ovarian
253 cancers (27,28). The top genes from TC247 were enriched for genes involved in proliferation
254 and immune cell activation, TC76 in replication stress, TC250 in extracellular matrix (ECM)
255 interactions, and TC146 in neurotransmitter signaling.

256 Intriguingly, the top 100 genes in TC121 revealed a co-functional cluster enriched for
257 genes involved in synaptic signaling, with the corresponding proteins reported to localize to
258 the synaptic membrane of neurons (Fig. 4). Among these were pre-synaptic protein
259 neurexin-1 (*NRXN1*) and its post-synaptic ligand leucine-rich repeat transmembrane protein
260 2 (*LRRTM2*), which regulates excitatory synapse formation (top 20 genes are described in
261 Supplementary Table S9, for more details: http://transcriptional-landscape-
262 ovarian.opendatainscience.net) (29,30). Furthermore, this co-functional cluster included

263 neuron-specific synaptic structure proteins, neurofilament light, and medium chain.
264 Moreover, genes encoding for potassium ion channel proteins integral to membrane
265 repolarization during synapse signal transduction carried high weights in TC121. These genes
266 included *KCNC1*, *KCNN2*, and *KCNIP1*(31–33). Several genes in TC121 encoded proteins
267 related to glutamate receptor signaling, including *GRIN2C* and *SLC7A10* (34). In line with this
268 proposed function, high activity of TC121 was observed in neuroblastoma cell lines but not
269 in ovarian or central nervous system cancer cell lines in the GDSC and CCLE datasets (Fig. 5A,
270 Supplementary Fig. S7, S8). In the GEO and TCGA datasets, high activity of TC121 was
271 observed in glioblastoma multiforme and lower-grade glioma but not in ovarian cancer
272 patient samples (Fig. 5B).
273
274 **Distinct cluster of patients from TCGA overlap with elevated activity of TC121**
275 To explore if pre-existing classifications of patients with ovarian cancer correspond to the
276 contrasting activities of the TCs, we investigated the classification provided by TCGA. TCGA
277 identified four optimal clusters describing the patients with ovarian cancer using
278 transcriptional profiles.(9) To explore associations between these clusters and TC activity,
279 we performed a Kruskal-Wallis test using TCGA sample data. Supplementary Fig. S9
280 highlights the associations between each cluster set and the TCs, represented by log-
281 transformed p-values. A significant association between a TC and a cluster set indicates that
282 at least one cluster within the cluster set exhibited significantly different activity scores for
283 the corresponding TC compared to the other clusters. Notably, samples with high TC121
284 activity were not captured by any of the clusters of the four-cluster set. Interestingly, the
285 eight-cluster set predefined by TCGA was able to identify a cluster that corresponded to
286 samples with elevated TC121 and TC146 activity. This finding suggests that while TCGA's

287 analysis identified this patient group based on transcriptional profiles, it didn't characterize
288 them further.
289
290 **Distinct spatial and single cell transcriptional profiles with high activity of OS-associated**
291 **TCs**
292 Cross-study TC projection onto spatial transcriptomic profiles from 11 ovarian cancer
293 samples revealed that TC121 was highly active in profiles from the tumor region of the 11
294 ovarian cancer samples (Fig. 6A; Supplementary Fig. S10). Additionally, TC121 showed
295 markedly higher activity in the transcriptional profiles of a subset of the unannotated single
296 cells from HGSOC patients (study ID GSE158722; see supplementary methods and
297 Supplementary Fig. S11).(35) This finding suggests that some of these unannotated cells
298 could be neurons. Furthermore, the unannotated single cell transcriptional profiles showed
299 contrasting activity scores of different OS-associated TCs (supplementary Fig. S11). These
300 contrasting activities indicate that these TCs could provide insights into the biology of
301 previously uncharacterized cell types. Distinct regions with high activity of the copy number
302 TCs (TC166, TC247, and TC76) in the HGSOC sample overlapped with the region containing
303 cancer cells, as expected. TC250, enriched for extracellular matrix interactions, was also
304 active in the stromal region. The strongest inverse colocalization (colocalization score -2.43)
305 was observed between the activity scores of TC146, enriched for neurotransmitter signaling,
306 and TC76, captured the effect of copy number alterations at chromosome 9p13-p21, at the
307 serous ovarian cancer sample (Fig. 6B, Supplementary Table S10).
308
309 **Discussion**

310 In this study, we identified 374 TCs, each enriched for gene sets representing various
311 biological processes in HGSOC samples. Six could stratify patients with HGSOC who had
312 received platinum-based treatment into ten distinct OS groups.

313 The most significant TC in the survival tree analysis, TC121, captured a clinically
314 relevant subtle transcriptional pattern linked to synaptic signaling not previously recognized
315 in HGSOC. In the survival tree, TC121 identified 12% of the HGSOC patients with the shortest
316 OS and, based on spatially resolved transcriptomic analyzed samples, is active in tumor
317 regions. This observation supports the emerging role of neurons and neuronal projections as
318 cancer hallmark-inducing constituents of the TME (36–38).

319 Further investigation on whether the activity of TC121 originated from tumor cells or
320 in the TME revealed that the TC121 signal is coming from cells within the TME. The high
321 activity of TC121 in low-grade glioma and glioblastoma multiforme patient samples (Fig. 5B)
322 is in agreement with the presence of neurons in large numbers within the TME of gliomas,
323 where they form functional synapses with tumor cells(39,40). Moreover, TC121 activity was
324 lower in non-brain cancers, such as ovarian cancers, which contain fewer neurons and
325 synapses in the TME compared to brain cancers. We expected TC121 activity to be low in the
326 bulk transcriptomes of all cell lines, since they lack TME. TC121 activity in most cell lines,
327 which includes glioblastoma and ovarian cancer cell lines, was indeed low. Neuroblastoma
328 cell lines, however, exhibited high TC121 activity, which is likely due to retained synaptic
329 formation capacity originating from neuroblast cells (41,42). Lastly, TC121's high activity
330 observed in small, scattered regions within the tumor of spatially resolved transcriptomic
331 ovarian cancer samples also supports TC121's role in the TME.

332 TC121's significant association with OS underscores the potential significance of
333 synaptic signaling in HGSOC biology. Yet, the neuronal subtype and the molecular

334 mechanisms associated with TC121 remain to be elucidated. A study in human ovarian
335 cancer-bearing mice demonstrated that sympathetic innervation in HGSOC involves
336 adrenergic signaling: norepinephrine released by sympathetic neurons binds to beta-
337 adrenergic receptors on the cancer cells (43–45). This binding triggers the tumor cells to
338 release brain-derived neurotrophic factor (BDNF), which enhances cancer innervation via
339 activation of host neurotrophic receptor tyrosine kinase B receptors (NTRK2), thereby
340 establishing a feed-forward loop of sustained signaling. BDNF and the nerve marker
341 neurofilament protein expression were examined in 108 human ovarian tumors (41). This
342 study revealed that increased intratumoral nerve presence strongly correlates with elevated
343 BDNF and norepinephrine levels, advanced tumor stage, and shorter OS in patients with
344 ovarian cancer. This interaction can be targeted with pan-TRK inhibitors such as entrectinib
345 and larotrectinib. Both drugs are showing promising results in multiple phase II trials,
346 including ovarian cancer and breast cancer patients. Furthermore, a TRKB-specific inhibitor
347 was developed (ANA-12), but has not been subjected to any clinical trials in cancer so far
348 (46–49). Our analysis indicated that *BDNF* is a prominent gene (with an absolute weight > 3)
349 in 10 TCs but not in TC121, suggesting that TC121 may indicate a distinct process unrelated
350 to BDNF.

351 The significance of sensory innervation in HGSOC was evidenced by the co-
352 localization of TRPV1, a marker for sensory neurons, and β-III tubulin, a general neuronal
353 marker, in immunofluorescent staining of histological sections from 75 patients (50).
354 Additionally, a murine model study employing neural tracing identified sensory neurons
355 originating from local dorsal root ganglia and jugular–nodose ganglia, with axons extending
356 into the TME (50). A transgenic murine model lacking nociceptors demonstrated that this
357 specific subtype of sensory neurons was involved in tumor progression (51). Another study

358 showed that reducing the release of Calcitonin gene-related peptide from tumor-innervating
359 nociceptors could be a strategy to alleviate this effect of nociceptors by improving anti-
360 tumour immunity of cytotoxic CD8+ T cells in a melanoma model bearing mice(52). This
361 indicates that the signal from TC121 may represent an indirect influence on tumor cells via
362 interactions with immune cells and the promotion of an immune suppressive TME.
363 Furthermore, in cell lines derived from Trp53$^{-/-}$ Pten$^{-/-}$ murine HGSOC, the influence of
364 nociceptors was characterized by the release of substance P (SP), their primary
365 neuropeptide. SP is an alternative splicing product of the preprotachykinin A gene (*TAC1*)
366 and binds to the receptor neurokinin 1 (NK1R), encoded by the *TACR1* gene. NK1R
367 expression was confirmed in murine HGSOC cell line, and SP enhanced cellular proliferation
368 in NK1R-positive murine HGSOC cancer cells *in vitro* (51). Our analysis identified *TAC1* and
369 *TACR1* as prominent genes in 15 and 2 TCs, respectively, yet not in TC121, and none of these
370 TCs were associated with patient survival. Currently, there are no drugs specifically targeting
371 tumor innervation in (ovarian) cancer (53). Interestingly, the NK1R antagonist aprepitant
372 effectively inhibited the metastasis-promoting effects of neural substance P in human breast
373 and mammary cancer bearing mice (54), demonstrating the feasibility of such an approach.
374 Strategies to disrupt neuronal signaling and neurotransmitter release in neurons target key
375 elements of excitatory neurotransmission, such as calcium flux and vesicle formation. Drugs
376 like ifenprodil and lamotrigine, commonly used to treat neuronal disorders, block glutamate
377 release and subsequent neuronal signaling. Additionally, the vesicular monoamine
378 transporter (VMAT) inhibitor reserpine prevents synaptic vesicle formation (55,56). In vitro
379 studies with HGSOC cell lines have demonstrated that ifenprodil significantly inhibits tumour
380 proliferation, while reserpine induces apoptosis in cancer cells (57,58). These approaches
381 hold promise for inhibiting neuronal signaling and interactions in the TME. Therefore, it is

382 essential that the mechanisms driving this nerve growth, the specifics of how nerves within
383 the TME interact with ovarian cancer cells, and how they impact the survival of patients with
384 HGSOC are further elucidated.

385 Altogether, the present study uncovered a clinically relevant TC linked to synaptic
386 signaling not previously identified in HGSOC. This TC may represent a novel cancer cell-
387 extrinsic mechanism within the TME, illustrating how cancer cells and nerve cells interact to
388 promote enhanced proliferation. A deeper understanding of the molecular aspects of tumor
389 innervation could pave the way for novel drug targets for patients with HGSOC.

390 Data availability

391 Microarray expression data was collected from three public data repositories: Gene
392 Expression Omnibus with accession number GPL570 (generated with Affymetrix HG-U133
393 Plus 2.0), CCLE (generated with Affymetrix HG-U133 Plus 2.0, file
394 CCLE_Expression.Arrays_2013-03-18.tar.gz) available at
395 https://portals.broadinstitute.org/ccle/data and GDSC (generated with Affymetrix HG-U219)
396 available at https://www.ebi.ac.uk/arrayexpress/experiments/E-MTAB-3610/. Pre-processed
397 and normalized RNA-seq data was collected from TCGA using the Broad GDAC Firehose
398 portal (https://gdac.broadinstitute.org/). Spatially resolved samples were sourced from
399 10xGenomics and GEO. The datasets generated during and/or analyzed during the current
400 study are available in the website: http://transcriptional-landscape-
401 ovarian.opendatainscience.net. The accession numbers of the studies included in this
402 analysis are mentioned in Supplementary Table S2.

403 Code Availability

404 The complete set of codes utilized in this study is available at the github repository:
405 https://github.com/arkajyotibhattacharya/TranscriptionalLandscapeOvarianCancer.

Funding

This research was supported by a Hanarth Fund grant, the Netherlands (2019N1552 to R.S.N.F).

Author contribution

A. Bhattacharya: Data curation, methodology, data analysis, data interpretation, writing. T. S. Stutvoet: Data curation, methodology, data analysis, data interpretation, writing. M. Perla: Data interpretation, writing. S. Loipfinger: Data analysis, data interpretation, writing. M. Jalving: Data interpretation, writing. A. K. L. Reyners: Data interpretation, writing. P. D. Vermeer: Data interpretation, writing. R. Drapkin: Data interpretation, writing. M. de Bruyn: Data interpretation, writing. E. G. E. de Vries: Data interpretation, writing. S. de Jong: Conceptualization, data interpretation, writing. R. S. N. Fehrmann: Conceptualization, data curation, methodology, data analysis, data interpretation, writing. All were involved in the final decision to submit the manuscript.

Disclosure

The authors have declared no conflicts of interest.

Figure legends

Figure 1. Workflow indicates the data acquisition and relations between the methods.

428 **Figure 2. Enrichment heatmap of hallmark gene sets in transcriptional components**
429 **associated with patient overall survival.** Gene Set Enrichment Analysis for 14 TCs associated
430 with OS identified through univariate or multivariate survival analyses are presented. Only
431 Hallmark gene sets with significant enrichment (Bonferroni-corrected p-value) for at least
432 one TC are shown. The heatmap displays Z-scores, which indicate the relative enrichment
433 strength, with values truncated at a maximum of 4 for visualization purposes. The gene sets
434 were clustered based on Pearson correlation using the Ward D2 method, providing insights
435 into related biological processes captured by different TCs. In the right column,
436 chromosomal locations of copy number alterations (CNAs) are shown, reflecting the
437 downstream effects on gene expression that each TC captures. This integration of CNA
438 information highlights the biological relevance of each TC and its contribution to gene
439 expression variability and patient outcomes.
440
441 **Figure 3. Survival tree analysis of patients with platinum-treated HGSOC defines survival**
442 **cohorts with distinct clinicopathologic and biological characteristics.** The results of survival
443 tree analysis of 294 patients with high-grade serous ovarian cancer (HGSOC) treated with
444 platinum-based chemotherapy are presented. The analysis utilized 14 transcriptional
445 components (TCs) associated with overall survival (OS), along with other clinicopathologic
446 factors, including age, tumor stage, grade, and debulking status. The resulting tree identified
447 nine distinct survival cohorts, each represented as a bar in the Sankey diagram, where the
448 bar height corresponds to the number of patients in each cohort. Kaplan-Meier survival
449 curves with accompanying number-at-risk tables are shown for each cohort, with survival
450 data censored at 10 years. The names of the survival cohorts were based on enriched
451 biological processes in the TCs, as determined by the chromosomal location of genes

452 captured by a TC, GSEA, and co-functionality analysis of the top genes. The p-values in the
453 Kaplan-Meier plots were derived from log-rank tests comparing survival distributions
454 between groups. Abbreviations: TC = transcriptional component, ECM = extracellular matrix.
455
456 **Figure 4. Co-functionality network of top 100 absolute weighted genes in TC121.** Co-
457 functionality network for the top 100 genes with the highest absolute weights in TC121 is
458 presented. Genes were clustered based on predicted co-functionality (r > 0.7) across
459 datasets, with clusters identified using both Gene Ontology (GO) Biological Processes and
460 Cellular Components databases. One primary cluster, containing more than five genes,
461 exhibited strong enrichment for synaptic signaling in the GO Biological Processes database
462 and for synaptic membranes in the GO Cellular Components database. This highlights the
463 biological specificity of TC121 in regulating gene expression linked to synaptic functions.
464
465 **Figure 5.** The activity of TC121 in bulk transcriptomes of CCLE, GDSC cell lines, and GEO and
466 TCGA patient-derived samples. **A.** Cross-study TC projection of TC121 on CCLE and GDSC cell
467 lines. The boxplots display the activity scores of TC121 in different tissue types, which are
468 ordered based on their corresponding median activity scores. **B**. Cross-study TC projection of
469 TC121 on GEO and TCGA bulk transcriptomes resulted in the activity scores presented in the
470 boxplots. Cancer types were ordered based on corresponding medians of TC121 activity
471 scores. Abbreviations: TC = transcriptional component.
472
473 **Figure 6.** Spatial transcriptomic profiles in ovarian cancer samples. **A.** We employed a
474 permutation-based approach to pinpoint the areas of significant TC activity in spatial
475 transcriptomic profiles. We ran 5,000 permutations for each TC-profile combination, yielding

476 a p-value that indicates the extent to which the TC activity in the corresponding profile
477 differs from what would be expected by chance (the null distribution). We then transformed
478 these p-values into logarithmic values and represented them using a heatmap. Heatmaps of
479 activity scores of the TCs are presented in individual rows for the HGSOC, serous papillary,
480 and endometrioid adenocarcinoma of ovary samples. The first column represents the
481 stained images of the samples. The second to seventh columns show heatmaps
482 corresponding to the mentioned TCs. **B.** The heatmap illustrates the colocalization between
483 two TC activities on spatial transcriptomic profiles from ovarian cancer samples. For each
484 cell, the colocalization scores of the TCs at each of the three spatial transcriptomics samples
485 OC 1, OC 2, and OC 3 are arranged in columns. A colocalization score of 4 between two TCs
486 (red) indicates that the positively (+) and negatively (-) active regions of both TCs are
487 perfectly colocalized. Conversely, a colocalization score of -4 between two TCs (blue) also
488 indicates colocalization. Still, with inverse activity, i.e., the positively active regions of one TC
489 are colocalized with the negatively active regions of the other TC or vice versa. A
490 colocalization score close to 0 between two TCs (white) indicates that the activities of two
491 TCs are spatially separated. The dashed and solid circle in the panel on the right side of the
492 color bar represents two different TCs. Abbreviations: TC = transcriptional component.
493
494 **Supplementary Figure S1.** Association of OS-related TCs with clinicopathologic parameters.
495 The association between clinicopathologic parameters and the activity of the OS-associated
496 14 TCs was determined in the complete set of 1,125 samples. Pearson correlation was used
497 to calculate the association of each clinicopathologic parameter with each TC. The TCs were
498 then ranked based on their association with OS. Abbreviations: TC = transcriptional
499 component, OS = overall survival.

500

501 **Supplementary Figure S2.** Enrichment heatmap for the KEGG gene set collection in OS-
502 related TCs. GSEA results of 14 TCs associated with OS in univariate or multivariate survival
503 analysis are presented, including KEGG gene sets that were included if the enrichment for at
504 least one TC passed the Bonferroni threshold for multiple testing correction. The gene sets
505 were clustered using Pearson correlation and Ward D2, and the heatmap colors were based
506 on Z-scores, truncated at a value of four. The right column shows the chromosomal location
507 of a copy number alteration that the TC captures the downstream effects on gene
508 expression levels. Abbreviations: TC = transcriptional component, OS = overall survival.

509

510 **Supplementary Figure S3.** Enrichment heatmap for the REACTOME gene set collection in OS-
511 related TCs. GSEA results of 14 TCs associated with OS in univariate or multivariate survival
512 analysis is presented, including REACTOME gene sets that were included if the enrichment
513 for at least one TC passed the Bonferroni threshold for multiple testing correction. The gene
514 sets were clustered using Pearson correlation and Ward D2, and the heatmap colors were
515 based on Z-scores, truncated at a value of four. The right column shows the chromosomal
516 location of a copy number alteration that the TC captures the downstream effects on gene
517 expression levels. Abbreviations: TC = transcriptional component.

518

519 **Supplementary Figure S4.** Survival tree analysis of patients with advanced-stage, HGSOC
520 defines survival cohorts with distinct clinicopathologic and biological characteristics. Survival
521 tree analysis of 265 patients with advanced-stage, platinum-treated HGSOC using 14 OS-
522 associated TCs and other classifiers such as age, tumor stage, grade, and debulking status.

523 The analysis resulted in nine survival cohorts, and the height of the bar in the Sankey
524 diagram represents the number of patients in each cohort. The Kaplan-Meier plots and
525 number-at-risk tables are presented with survival data censored at 10 years. The names of
526 the survival cohorts were based on enriched biological processes in the TCs, as determined
527 by the chromosomal location of genes captured by a TC, GSEA, and co-functionality analysis
528 of the top genes. The p-values in each panel show the p-value from the corresponding log-
529 rank test between the two groups. Abbreviations: TC = transcriptional component, ECM =
530 extracellular matrix.

531

532 **Supplementary Figure S5.** The activity of TC121 in bulk transcriptomes of patients with
533 different subtypes of ovarian cancer. The boxplots display the activity scores of TC121 in
534 different cancer subtypes, which are ordered based on their corresponding median activity
535 scores.

536

537 **Supplementary Figure S6.** Three OS-associated TCs capture the transcriptional effect of copy
538 number alterations. For each OS-related TC, the weight of each gene was plotted on its
539 genomic location. Abbreviations: TC = transcriptional component.

540

541 **Supplementary Figure S7**. Activity of OS-associated TCs in bulk transcriptomes of CCLE cell
542 lines. The proportion of samples with outlier activity scores in individual tissue types for each
543 of the 14 OS-associated TCs was obtained using an absolute cut-off value of 0.05. TCs were
544 ordered based on their association with OS. Abbreviations: TC = transcriptional component.

545

546 **Supplementary Figure S8**. The activity of OS-associated TCs in bulk transcriptomes of GDSC
547 cell lines. The proportion of samples with outlier activity scores in individual tissue types for
548 each of the 14 OS-associated TCs was obtained using an absolute cut-off value of 0.05. TCs
549 were ordered based on their association with OS. Abbreviations: TC = transcriptional
550 component.

551

552 **Supplementary Figure S9.** Association heatmap for the TCGA cluster-sets with the activity
553 scores of OS-related TCs. This heatmap highlights the associations between each cluster set
554 and the TCs, represented by log-transformed p-values from corresponding Kruskal-Wallis
555 test. A significant association between a TC and a cluster set indicates that at least one
556 cluster within the cluster set exhibited significantly different activity scores for the
557 corresponding TC compared to the other clusters. The heatmap colors were based on log-
558 transformed p-values. Abbreviations: TC = transcriptional component. OS = overall survival.

559

560 **Supplementary Figure S10**. Spatial transcriptomic profiles in eight ovarian cancer samples.
561 **A.** We employed a permutation-based approach to pinpoint the areas of significant TC
562 activity in spatial transcriptomic profiles. We ran 5,000 permutations for each TC-profile
563 combination, yielding a p-value that indicates the extent to which the TC activity in the
564 corresponding profile differs from what would be expected by chance (the null distribution).
565 We then transformed these p-values into logarithmic values and represented them using a
566 heatmap. Heatmaps of activity scores of the TCs are presented in individual rows for the
567 HGSOC samples. The first column represents the stained images of the samples. The second
568 to seventh columns show heatmaps corresponding to the mentioned TCs. **B.** The heatmap

569 illustrates the colocalization between two TC activities on spatial transcriptomic profiles
570 from ovarian cancer samples. For each cell, the colocalization scores of the TCs at each of
571 the eight spatial transcriptomics samples are arranged in columns. A colocalization score of 4
572 between two TCs (red) indicates that the positively (+) and negatively (-) active regions of
573 both TCs are perfectly colocalized. Conversely, a colocalization score of -4 between two TCs
574 (blue) also indicates colocalization. Still, with inverse activity, i.e., the positively active
575 regions of one TC are colocalized with the negatively active regions of the other TC or vice
576 versa. A colocalization score close to 0 between two TCs (white) indicates that the activities
577 of two TCs are spatially separated. The dashed and solid circle in the panel on the right side
578 of the color bar represents two different TCs. Abbreviations: TC = transcriptional component.
579
580 **Supplementary Figure 11.** The activity scores of OS-associated TCs in different single cell
581 types from patients with HGSOC. Abbreviations: TC = transcriptional component. OS =
582 overall survival. HGSOC = high-grade serous ovarian cancer.
583

584 **Supplementary table legends**

585 **Supplementary Table S1.** Patient characteristics. Abbreviations: NA = not applicable, HGSOC
586 = high-grade serous ovarian cancer, LGSOC = low-grade serous ovarian cancer, LMP = low
587 malignant potential, OCCC = ovarian clear cell cancer.

588

589 **Supplementary Table S2.** Overview of the number of samples from each GEO series and the
590 corresponding study. Abbreviations: PMID = PubMed identification number.

591

592 **Supplementary Table S3.** Multivariate permutation framework results from the univariate
593 survival analysis. Abbreviations: TC = transcriptional component. CI = confidence interval

594

595 **Supplementary Table S4.** Permutation framework results from the multivariate survival
596 analysis. Abbreviations: TC = transcriptional component. CI = confidence interval

597

598 **Supplementary Table S5.** Clinicopathological parameters per survival tree node in platinum-
599 treated HGSOC. Abbreviations: HGSOC = high-grade serous ovarian cancer, TC =
600 transcriptional component, ECM = extracellular matrix.

601

602 **Supplementary Table S6.** Clinicopathological parameters per survival tree node in advanced-
603 stage platinum-treated HGSOC. Abbreviations: HGSOC = high-grade serous ovarian cancer,
604 TC = transcriptional component, ECM = extracellular matrix.

605

606 **Supplementary Table S7.** GenetICA gene network analysis results. Abbreviations: TC =
607 transcriptional component.

608

609 **Supplementary Table S8.** Results from the univariate survival analysis on patients with

610 ovarian clear cell carcinoma. Abbreviations: TC = transcriptional component. CI = confidence

611 interval.

612

613 **Supplementary Table S9.** Expression and function of the top 20 genes in TC121, according to

614 literature. Abbreviations: TC = transcriptional component.

615

616 **Supplementary Table S10.** Colocalization scores of every two TC combinations in spatial

617 transcriptomic profiles from three ovarian cancer samples. Abbreviations: TC =

618 transcriptional component.

619 **References**

620

621 1. Lheureux S, Gourley C, Vergote I, Oza AM. Epithelial ovarian cancer. *Lancet*
622 2019;393:1240–53.

623 2. NCCN clinical practice guidelines in oncology - ovarian cancer, including fallopian tube
624 cancer and primary peritoneal cancer. November 26, 2019.

625 3. Wright AA, Bohlke K, Armstrong DK, Bookman MA, Cliby WA, Coleman RL, et al.
626 Neoadjuvant chemotherapy for newly diagnosed, advanced ovarian cancer: Society of
627 Gynecologic Oncology and American Society of Clinical Oncology Clinical Practice Guideline. *J*
628 *Clin Oncol* 2016;34:3460–73.

629 4. Corrado G, Salutari V, Palluzzi E, Distefano MG, Scambia G, Ferrandina G. Optimizing
630 treatment in recurrent epithelial ovarian cancer. *Expert Rev Anticancer Ther* 2017;17:1147–
631 58.

632 5. Cibula D, Balmaña J. PARP inhibitors in ovarian cancer. *Ann Oncol* 2016;27:i40–44.

633 6. Wang H, Xu T, Zheng L, Li G. Angiogenesis inhibitors for the treatment of ovarian cancer.
634 *Int J Gynecol Cancer* 2018;28:903–14.

635 7. Wu SG, Wang J, Sun JY, He ZY, Zhang WW, Zhou J. Real-world impact of survival by period
636 of diagnosis in epithelial ovarian cancer between 1990 and 2014. *Front Oncol* 2019;9:639.

637 8. Tewari KS, Burger RA, Enserro D, Norquist BM, Swisher EM, Brady MF, et al. Final overall
638 survival of a randomized trial of Bevacizumab for primary treatment of ovarian cancer. *J Clin*
639 *Oncol* 2019;37:2317–28.

640 9. Bell D, Berchuck A, Birrer M, Chien J, Cramer DW, Dao F, et al. Integrated genomic
641 analyses of ovarian carcinoma. *Nature* 2011;474:609–15.

642 10. Tothill RW, Tinker AV, George J, Brown R, Fox SB, Lade S, et al. Novel molecular subtypes
643 of serous and endometrioid ovarian cancer linked to clinical outcome. *Clin Cancer Res*
644 2008;14:5198–208.

645 11. Verhaak RGW, Tamayo P, Yang JY, Hubbard D, Zhang H, Creighton CJ, et al. Prognostically
646 relevant gene signatures of high-grade serous ovarian carcinoma. *J Clin Investig*
647 2013;123:517–25.

648 12. Chen C, Grennan K, Badner J, Zhang D, Gershon E, Jin L, et al. Removing batch effects in
649 analysis of expression microarray data: an evaluation of six batch adjustment methods. *PLoS*
650 *One* 2011;6:e17238.

651 13. Kong W, Vanderburg CR, Gunshin H, Rogers JT, Huang X. A review of independent
652 component analysis application to microarray gene expression data. *BioTechniques*
653 2008;45:501–20.

654 14. Chiappetta P, Roubaud MC, Torrsani B. Blind source separation and the analysis of
655 microarray data. *J Comput Biol* 2004;11:1090–109.

656 15. Biton A, Bernard-Pierrot I, Lou Y, Krucker C, Chapeaublanc E, Rubio-Pérez C, et al.
657 Independent component analysis uncovers the landscape of the bladder tumor
658 transcriptome and reveals insights into luminal and basal subtypes. *Cell Rep* 2014;9:1235–45.

659 16. Clough E, Barrett T. Statistical genomics, methods and protocols. *Methods Mol Biol*
660 2016;1418:93–110.

661 17. Fehrmann RSN, Karjalainen JM, Krajewska M, Westra H-J, Maloney D, Simeonov A, et al.
662 Gene expression analysis identifies global gene dosage sensitivity in cancer. *Nat Genet*
663 2015;47:115–25.

664 18. Barretina J, Caponigro G, Stransky N, Venkatesan K, Margolin AA, Kim S, et al. The cancer
665 cell line encyclopedia enables predictive modelling of anticancer drug sensitivity. *Nature*
666 2012;483:603–7.

667 19. Yang W, Soares J, Greninger P, Edelman EJ, Lightfoot H, Forbes S, et al. Genomics of drug
668 sensitivity in Cancer (GDSC): a resource for therapeutic biomarker discovery in cancer cells.
669 *Nucleic Acids Res* 2013;41:D955–61.

670 20. Barrett T, Wilhite SE, Ledoux P, Evangelista C, Kim IF, Tomashevsky M, et al. NCBI GEO:
671 archive for functional genomics data sets—update. *Nucleic Acids Res* 2013;41:D991–5.

672 21. Bhattacharya A, Bense RD, Urzúa-Traslaviña CG, de Vries EGE, van Vugt MATM,
673 Fehrmann RSN. Transcriptional effects of copy number alterations in a large set of human
674 cancers. *Nat Commun* 2020;11:715.

675 22. Subramanian A, Tamayo P, Mootha VK, Mukherjee S, Ebert BL, Gillette MA, et al. Gene
676 set enrichment analysis: a knowledge-based approach for interpreting genome-wide
677 expression profiles. *Proc Natl Acad Sci* 2005;102:15545–50.

678 23. Köhler S, Carmody L, Vasilevsky N, Jacobsen JOB, Danis D, Gourdine J-P, et al. Expansion
679 of the human phenotype ontology (HPO) knowledge base and resources. *Nucleic Acids Res*
680 2019;47(D1):D1018-D1027.

681 24. Urzúa-Traslaviña CG, Leeuwenburgh VC, Bhattacharya A, Loipfinger S, van Vugt MATM,
682 de Vries EGE , et al. Improving gene function predictions using independent transcriptional
683 components. *Nat Commun* 2021;12:1464.

684 25. Canozo FJG, Zuo Z, Martin JF, Samee MdAH. Cell-type modeling in spatial transcriptomics
685 data elucidates spatially variable colocalization and communication between cell-types in
686 mouse brain. *Cell Syst* 2022;13:58-70.e5.

687 26. Bolton KL, Chen D, Fuente RIC de la, Fu Z, Murali R, Kbel M, et al. Molecular subclasses of
688 clear cell ovarian carcinoma and their impact on disease behavior and outcomes. *Clin Cancer*
689 *Res* 2022;28:4947–56.

690 27. Huang RY, Chen GB, Matsumura N, Lai HC, Mori S, Li J, et al. Histotype-specific copy-
691 number alterations in ovarian cancer. *BMC Méd Genom* 2012;5:47.

692 28. Jongsma APM, Piek JMJ, Zweemer RP, Verheijen RHM, Gebbinck JWTK, Kamp GJ van, et
693 al. Molecular evidence for putative tumour suppressor genes on chromosome 13q specific to
694 BRCA1 related ovarian and fallopian tube cancer. *Mol Pathol* 2002;55:305.

695 29. Ko J, Fuccillo MV, Malenka RC, Südhof TC. LRRTM2 functions as a neurexin ligand in
696 promoting excitatory synapse formation. *Neuron* 2009;64:791–8.

697 30. de Wit J, Sylwestrak E, O'Sullivan ML, Otto S, Tiglio K, Savas JN, et al. LRRTM2 interacts
698 with neurexin1 and regulates excitatory synapse formation. *Neuron* 2009;64:799–806.

699 31. Ried T, Rudy B, Miera EV-S de, Lau D, Ward DC, Sen K. Localization of a highly conserved
700 human potassium channel gene (NGK2-KV4; KCNC1) to chromosome 11p15. *Genomics*
701 1993;15:405–11.

702 32. Willis M, Trieb M, Leitner I, Wietzorrek G, Marksteiner J, Knaus H-G. Small-conductance
703 calcium-activated potassium type 2 channels (SK2, KCa2.2) in human brain. *Brain Struct*
704 *Funct* 2017;222:973–9.

705 33. Bourdeau ML, Laplante I, Laurent CE, Lacaille JC. KChIP1 modulation of Kv4.3-mediated
706 A-type K+ currents and repetitive firing in hippocampal interneurons. *Neuroscience*
707 2011;176:173–87.

708 34. Ehmsen JT, Liu Y, Wang Y, Paladugu N, Johnson AE, Rothstein JD, et al. The astrocytic
709 transporter SLC7A10 (Asc-1) mediates glycinergic inhibition of spinal cord motor neurons. *Sci*
710 *Rep* 2016;6:35592.

711 35. Nath A, Cosgrove PA, Mirsafian H, Christie EL, Pflieger L, Copeland B, et al. Evolution of
712 core archetypal phenotypes in progressive high grade serous ovarian cancer. *Nat Commun*
713 2021;12:3039.

714 36. Hanahan D, Weinberg RA. Hallmarks of cancer: the next generation. *Cell* 2011;144:646–
715 74.

716 37. Reavis HD, Chen HI, Drapkin R. Tumor Innervation: Cancer Has Some Nerve. *Trends*
717 *Cancer* 2020;6:1059–67.

718 38. Gysler SM, Drapkin R. Tumor innervation: peripheral nerves take control of the tumor
719 microenvironment. *J Clin Investig* 2021;131:e147276.

720 39. Radin DP, Tsirka SE. Interactions between tumor cells, neurons, and microglia in the
721 glioma microenvironment. *Int J Mol Sci* 2020;21:8476.

722 40. Venkatesh HS, Morishita W, Geraghty AC, Silverbush D, Gillespie SM, Arzt M, et al.
723 Electrical and synaptic integration of glioma into neural circuits. *Nature* 2019;573:539–45.

724 41. Preter KD, Vandesompele J, Heimann P, Yigit N, Beckman S, Schramm A, et al. Human
725 fetal neuroblast and neuroblastoma transcriptome analysis confirms neuroblast origin and
726 highlights neuroblastoma candidate genes. *Genome Biol* 2006;7:R84.

727 42. Mark B, Lai S-L, Zarin AA, Manning L, Pollington HQ, Litwin-Kumar A, et al. A
728 developmental framework linking neurogenesis and circuit formation in the Drosophila CNS.
729 *eLife* 2021;10:e67510.

730 43. Allen JK, Armaiz-Pena GN, Nagaraja AS, Sadaoui NC, Ortiz T, Dood R, et al. Sustained
731 adrenergic signaling promotes intratumoral innervation through BDNF induction. *Cancer Res*
732 2018;78:3233-3242.

733 44. Rains SL, Amaya CN, Bryan BA. Beta-adrenergic receptors are expressed across diverse
734 cancers. *Oncoscience* 2017;4:95–105.

735 45. Eng JWL, Kokolus KM, Reed CB, Hylander BL, Ma WW, Repasky EA. A nervous tumor
736 microenvironment: the impact of adrenergic stress on cancer cells, immunosuppression, and
737 immunotherapeutic response. *Cancer Immunol Immunother* 2014;63:1115–28.

738 46. Drilon A, Siena S, Ou S-HI, Patel M, Ahn MJ, Lee J, et al. Safety and antitumor activity of
739 the multitargeted Pan-TRK, ROS1, and ALK inhibitor entrectinib: combined results from two
740 phase I trials (ALKA-372-001 and STARTRK-1). *Cancer Discov* 2017;7:400–9.

741 47. Ardini E, Menichincheri M, Banfi P, Bosotti R, Ponti CD, Pulci R, et al. Entrectinib, a pan–
742 TRK, ROS1, and ALK inhibitor with activity in multiple molecularly defined cancer indications.
743 *Mol Cancer Ther* 2016;15:628–39.

744 48. Drilon A, Laetsch TW, Kummar S, DuBois SG, Lassen UN, Demetri GD, et al. Efficacy of
745 larotrectinib in TRK fusion–positive cancers in adults and children. *N Engl J Med*
746 2018;378:731–9.

747 49. Burris HA, Shaw AT, Bauer TM, Farago AF, Doebele RC, Smith S, et al. Abstract 4529:
748 Pharmacokinetics (PK) of LOXO-101 during the first-in-human phase I study in patients with
749 advanced solid tumors: Interim update. *Cancer Res* 2015;75:4529–4529.

750 50. Barr JL, Kruse A, Restaino AC, Tulina N, Stuckelberger S, Vermeer SJ, et al. Intra-tumoral
751 nerve-tracing in a novel syngeneic model of high-grade serous ovarian carcinoma. Cells
752 2021;10:3491.

753 51. Restaino AC, Walz A, Vermeer SJ, Barr J, Kovács A, Fettig RR, et al. Functional neuronal
754 circuits promote disease progression in cancer. Sci Adv 2023;9:eade4443.

755 52. Balood M, Ahmadi M, Eichwald T, Ahmadi A, Majdoubi A, Roversi K, et al. Nociceptor
756 neurons affect cancer immunosurveillance. Nature. 2022;611:405–12.

757 53. Li X, Peng X, Yang S, Wei S, Fan Q, Liu J, et al. Targeting tumor innervation: premises,
758 promises, and challenges. Cell Death Discov 2022;8:131.

759 54. Padmanaban V, Keller I, Seltzer ES, Ostendorf BN, Kerner Z, Tavazoie SF. Neuronal
760 substance-P drives breast cancer growth and metastasis via an extracellular RNA-TLR7 axis.
761 bioRxiv 2024;2024.03.08.584128.

762 55. Williams K. Ifenprodil, a novel NMDA receptor antagonist: site and mechanism of
763 action. *Curr Drug Targets* 2001;2:285–98.

764 56. Reid JG, Gitlin MJ, Altshuler LL. Lamotrigine in psychiatric disorders. *J Clin Psychiatry*
765 2013;74:675–84.

766 57. Ramamoorthy MD, Kumar A, Ayyavu M, Dhiraviam KN. Reserpine induces apoptosis and
767 cell cycle arrest in hormone independent prostate cancer cells through mitochondrial
768 membrane potential failure. *Anti-Cancer Agents Med Chem* 2019;18:1313–22.

769 58. North WG, Liu F, Tian R, Abbasi H, Akerman B. NMDA receptors are expressed in human
770 ovarian cancer tissues and human ovarian cancer cell lines. *Clin Pharmacol: Adv Appl*
771 2015;7:111–7.

772

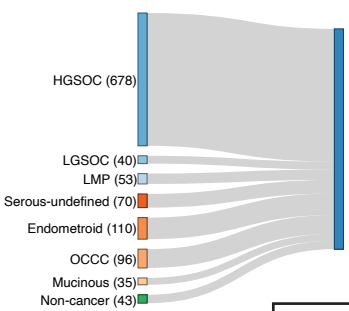

bulk transcriptomics (n = 1,125)

$$\begin{bmatrix} x_1 \\ x_2 \\ \vdots \\ x_n \end{bmatrix}$$

Consensus independent component analysis

$f(u) = \log \cosh(u)$

Mixing matrix (TC activity per sample)

$$\begin{bmatrix} \hat{a}_{11} & \hat{a}_{21} & \cdots & \hat{a}_{n1} \\ \hat{a}_{12} & \hat{a}_{22} & \cdots & \hat{a}_{n2} \\ \vdots & \vdots & & \vdots \\ \hat{a}_{1m} & \hat{a}_{2m} & \cdots & \hat{a}_{nm} \end{bmatrix}$$

Transcriptional components (Gene weights in TC)

$$\begin{bmatrix} \hat{s}_1 \\ \hat{s}_2 \\ \vdots \\ \hat{s}_m \end{bmatrix}$$

Cox proportional hazards analysis for OS

Univariate

TC activity scores

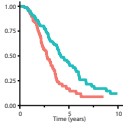

Multivariate

TC activity scores
Age
Stage
Grade
Debulking status

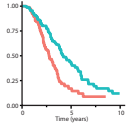

TCs significantly associated with OS after multiple testing correction

Survival tree analysis on platinum treated serous ovarian cancer patients

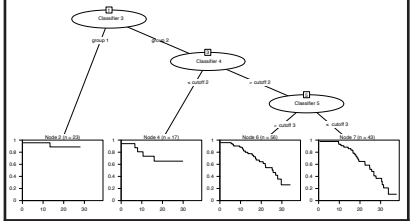

Robustness analysis using permutations

Identification of biological processes related to clinical outcome

TC activity↑

↓

Expression of genes in biological processes↑

↓

Overall survival↓

Association with biological processes

GenetICA-Network analysis

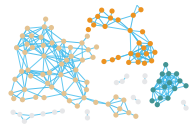

Geneset enrichment analysis on 16 geneset databases

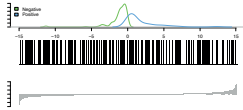

Copy number detection

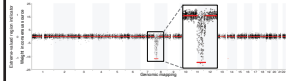

Cross-study TC projection

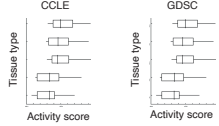

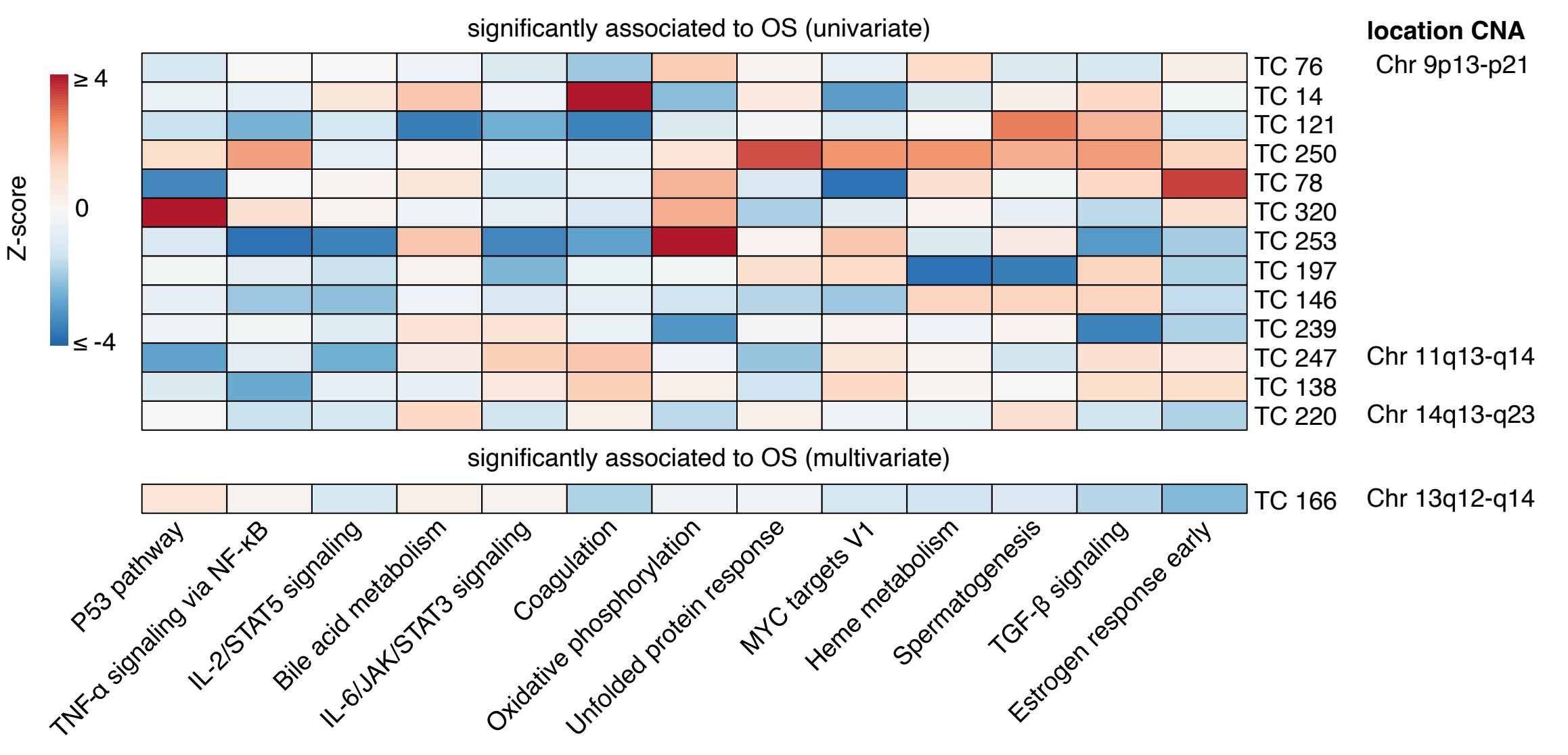
significantly associated to OS (univariate)
location CNA
Z-score
≥ 4
0
≤ -4
TC 76
TC 14
TC 121
TC 250
TC 78
TC 320
TC 253
TC 197
TC 146
TC 239
TC 247
TC 138
TC 220
Chr 9p13-p21
Chr 11q13-q14
Chr 14q13-q23
significantly associated to OS (multivariate)
TC 166
Chr 13q12-q14
P53 pathway
TNF-α signaling via NF-κB
IL-2/STAT5 signaling
Bile acid metabolism
IL-6/JAK/STAT3 signaling
Coagulation
Oxidative phosphorylation
Unfolded protein response
MYC targets V1
Heme metabolism
Spermatogenesis
TGF-β signaling
Estrogen response early

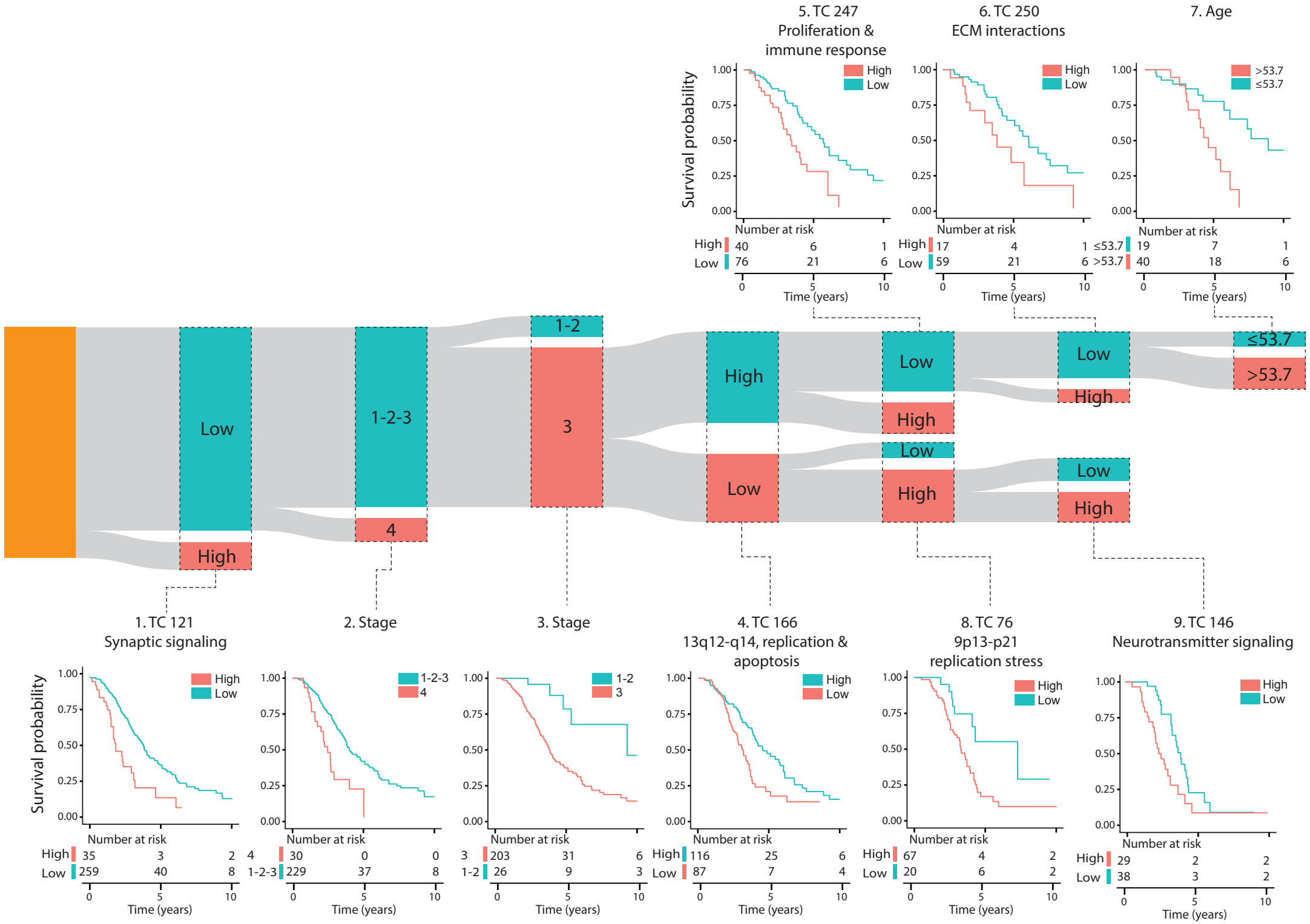
5. TC 247
Proliferation &
immune response
6. TC 250
ECM interactions
7. Age
Survival probability
High
Low
>53.7
≤53.7
Number at risk
High 40 6 1
Low 76 21 6
High 17 4 1
Low 59 21 6
≤53.7 19 7 1
>53.7 40 18 6
Time (years)
1-2
1-2-3
3
4
High
Low
1. TC 121
Synaptic signaling
2. Stage
3. Stage
4. TC 166
13q12-q14, replication &
apoptosis
8. TC 76
9p13-p21
replication stress
9. TC 146
Neurotransmitter signaling
High 35 3 2
Low 259 40 8
4 30 0 0
1-2-3 229 37 8
3 203 31 6
1-2 26 9 3
High 116 25 6
Low 87 7 4
High 67 4 2
Low 20 6 2
High 29 2 2
Low 38 3 2

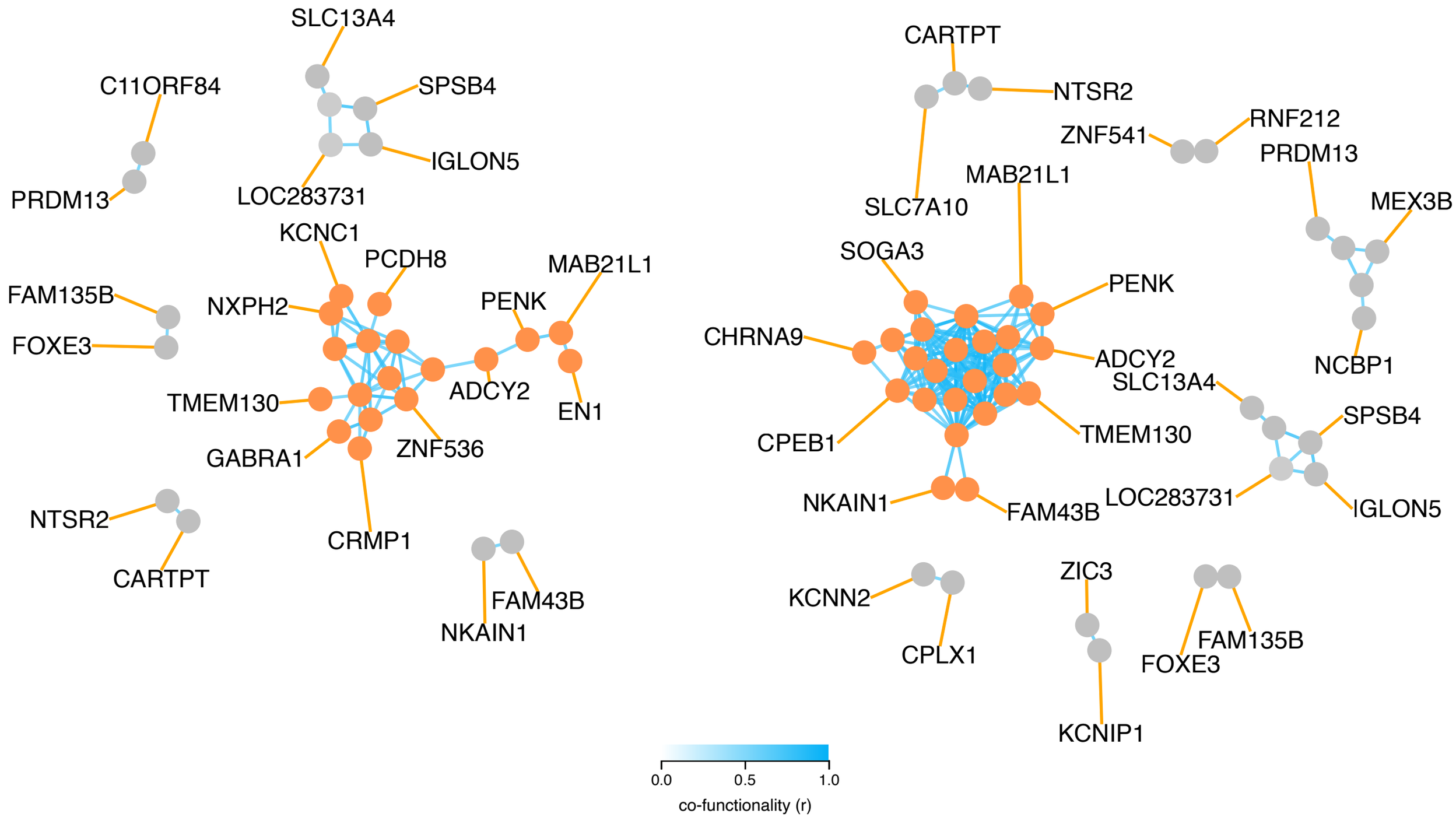

Z-score Gene Ontology biological processes genesets

- 11.5 - Synaptic signaling
- 10.3 - Modulation of synaptic transmission
- 9.51 - Single organism behavior
- 8.78 - Adult behavior
- 8.09 - Regulation of synaptic plasticity
- 7.69 - Cognition
- 7.47 - Glutamate receptor signaling
- 7.35 - Regulation of synaptic structure
- 7.34 - Behavior
- 7.12 - Regulation of neurotransmitter

Z-score Gene Ontology cellular components genesets

- 8.33 - Synaptic membrane
- 8.00 - Presynapse
- 7.72 - Postsynapse
- 7.61 - Postsynaptic membrane
- 7.57 - Presynaptic membrane
- 7.57 - Presynaptic active zone
- 7.43 - Transporter complex
- 7.08 - Potassium channel complex
- 7.07 - AMPA Glutamate receptor complex
- 7.03 - Cation channel complex

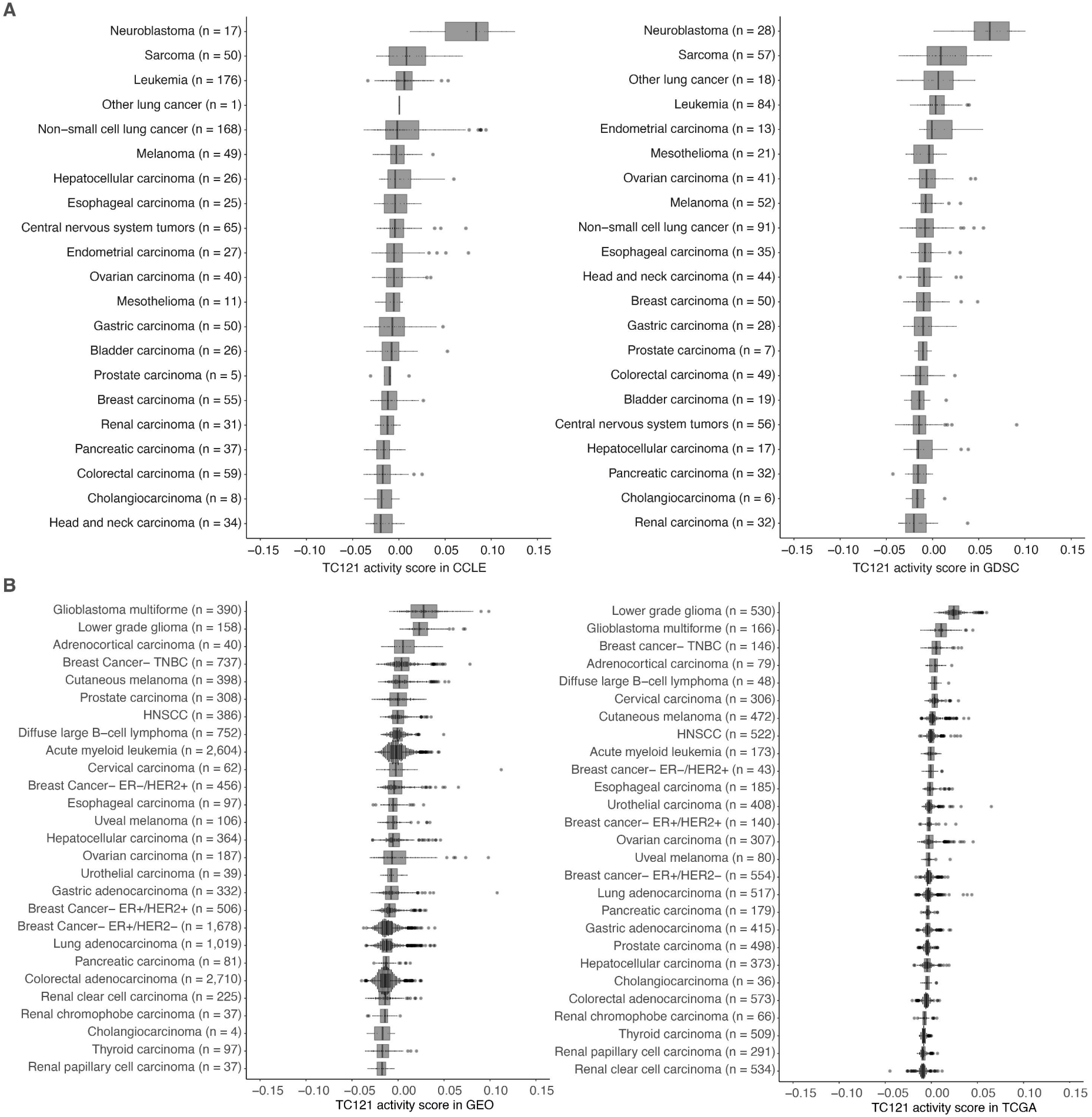
A
Neuroblastoma (n = 17)
Sarcoma (n = 50)
Leukemia (n = 176)
Other lung cancer (n = 1)
Non−small cell lung cancer (n = 168)
Melanoma (n = 49)
Hepatocellular carcinoma (n = 26)
Esophageal carcinoma (n = 25)
Central nervous system tumors (n = 65)
Endometrial carcinoma (n = 27)
Ovarian carcinoma (n = 40)
Mesothelioma (n = 11)
Gastric carcinoma (n = 50)
Bladder carcinoma (n = 26)
Prostate carcinoma (n = 5)
Breast carcinoma (n = 55)
Renal carcinoma (n = 31)
Pancreatic carcinoma (n = 37)
Colorectal carcinoma (n = 59)
Cholangiocarcinoma (n = 8)
Head and neck carcinoma (n = 34)
−0.15 −0.10 −0.05 0.00 0.05 0.10 0.15
TC121 activity score in CCLE
Neuroblastoma (n = 28)
Sarcoma (n = 57)
Other lung cancer (n = 18)
Leukemia (n = 84)
Endometrial carcinoma (n = 13)
Mesothelioma (n = 21)
Ovarian carcinoma (n = 41)
Melanoma (n = 52)
Non−small cell lung cancer (n = 91)
Esophageal carcinoma (n = 35)
Head and neck carcinoma (n = 44)
Breast carcinoma (n = 50)
Gastric carcinoma (n = 28)
Prostate carcinoma (n = 7)
Colorectal carcinoma (n = 49)
Bladder carcinoma (n = 19)
Central nervous system tumors (n = 56)
Hepatocellular carcinoma (n = 17)
Pancreatic carcinoma (n = 32)
Cholangiocarcinoma (n = 6)
Renal carcinoma (n = 32)
−0.15 −0.10 −0.05 0.00 0.05 0.10 0.15
TC121 activity score in GDSC
B
Glioblastoma multiforme (n = 390)
Lower grade glioma (n = 158)
Adrenocortical carcinoma (n = 40)
Breast Cancer− TNBC (n = 737)
Cutaneous melanoma (n = 398)
Prostate carcinoma (n = 308)
HNSCC (n = 386)
Diffuse large B−cell lymphoma (n = 752)
Acute myeloid leukemia (n = 2,604)
Cervical carcinoma (n = 62)
Breast Cancer− ER−/HER2+ (n = 456)
Esophageal carcinoma (n = 97)
Uveal melanoma (n = 106)
Hepatocellular carcinoma (n = 364)
Ovarian carcinoma (n = 187)
Urothelial carcinoma (n = 39)
Gastric adenocarcinoma (n = 332)
Breast Cancer− ER+/HER2+ (n = 506)
Breast Cancer− ER+/HER2− (n = 1,678)
Lung adenocarcinoma (n = 1,019)
Pancreatic carcinoma (n = 81)
Colorectal adenocarcinoma (n = 2,710)
Renal clear cell carcinoma (n = 225)
Renal chromophobe carcinoma (n = 37)
Cholangiocarcinoma (n = 4)
Thyroid carcinoma (n = 97)
Renal papillary cell carcinoma (n = 37)
−0.15 −0.10 −0.05 0.00 0.05 0.10 0.15
TC121 activity score in GEO
Lower grade glioma (n = 530)
Glioblastoma multiforme (n = 166)
Breast cancer− TNBC (n = 146)
Adrenocortical carcinoma (n = 79)
Diffuse large B−cell lymphoma (n = 48)
Cervical carcinoma (n = 306)
Cutaneous melanoma (n = 472)
HNSCC (n = 522)
Acute myeloid leukemia (n = 173)
Breast cancer− ER−/HER2+ (n = 43)
Esophageal carcinoma (n = 185)
Urothelial carcinoma (n = 408)
Breast cancer− ER+/HER2+ (n = 140)
Ovarian carcinoma (n = 307)
Uveal melanoma (n = 80)
Breast cancer− ER+/HER2− (n = 554)
Lung adenocarcinoma (n = 517)
Pancreatic carcinoma (n = 179)
Gastric adenocarcinoma (n = 415)
Prostate carcinoma (n = 498)
Hepatocellular carcinoma (n = 373)
Cholangiocarcinoma (n = 36)
Colorectal adenocarcinoma (n = 573)
Renal chromophobe carcinoma (n = 66)
Thyroid carcinoma (n = 509)
Renal papillary cell carcinoma (n = 291)
Renal clear cell carcinoma (n = 534)
−0.15 −0.10 −0.05 0.00 0.05 0.10 0.15
TC121 activity score in TCGA

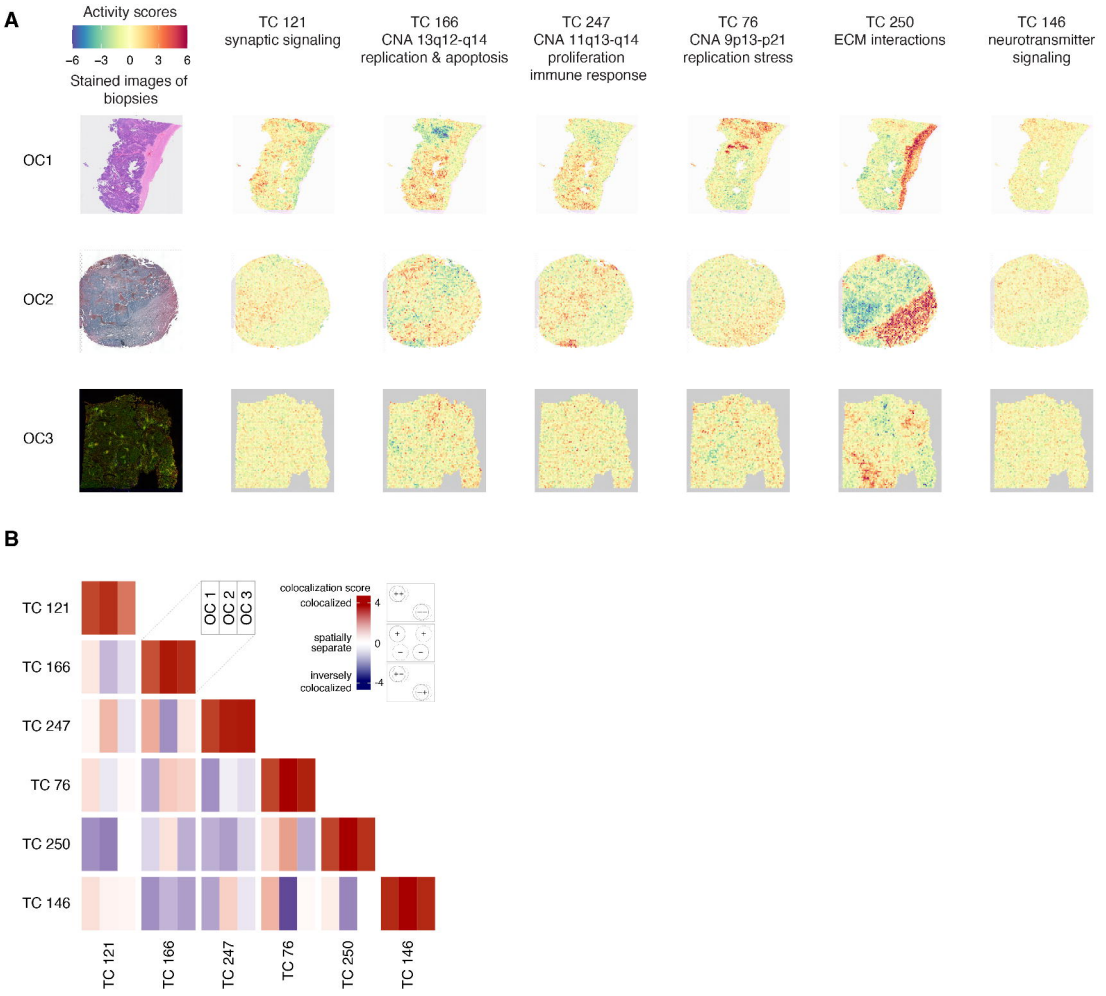
A
Activity scores
−6 −3 0 3 6
Stained images of biopsies
TC 121
synaptic signaling
TC 166
CNA 13q12-q14
replication & apoptosis
TC 247
CNA 11q13-q14
proliferation
immune response
TC 76
CNA 9p13-p21
replication stress
TC 250
ECM interactions
TC 146
neurotransmitter signaling
OC1
OC2
OC3
B
TC 121
TC 166
TC 247
TC 76
TC 250
TC 146
OC 1
OC 2
OC 3
colocalization score
colocalized
4
spatially separate
0
inversely colocalized
-4